# Kinetics of Low Reynolds Number Creaming and Coalescence in Droplet Dispersions

**S. A. K. Jeelani, R. Hosig, and E. J. Windhab**
Laboratory of Food Process Engineering, Institute of Food Science and Nutrition, Swiss Federal Institute of Technology, ETH-Technopark, 8005-Zurich, Switzerland

*DOI 10.1002/aic.10283*
*Published online in Wiley InterScience (www.interscience.wiley.com).*

*The effect of size distribution and concentration of rapeseed oil drops on the kinetics of creaming, and interdrop and interfacial coalescence in surfactant-free dispersions, in which the droplet Reynolds number for creaming is very small, is investigated. The concentration profiles of oil drops within the dispersion, measured using a radioactive $\gamma$-ray attenuation technique, show that the low Reynolds number of creaming small drops causes the dispersion to remain essentially loosely packed with drops during most of the time period. The creaming velocity and coalescence rate increase initially with time because of an increase in drop size by interdrop coalescence and decrease subsequently as larger drops cream out of the dispersion. Drops in concentrated dispersions, in which their mean diameter and concentration are large, grow in size faster, resulting in creaming and interfacial coalescence rates that are larger than those for dilute dispersions. An analytical model is presented that describes well not only the present experimental data on concentrated dispersions but also those published on very dilute dispersions. The results obtained by the model are in good agreement with those presented by other authors using the population balance model involving extensive numerical computations. The present model also enables the determination of coalescence times of single drops with their bulk homophase using experimental data on dispersions. These coalescence times, which decrease with increasing drop diameter, agree well with those predicted by the published equation for drainage of the continuous phase film between a spherical drop and its bulk homophase. The droplet capillary numbers are found to be very small, indicating that the drops are spherical in shape.*  *AIChE J,* 51: 149–161, 2005
*Keywords: coalescence, creaming, dispersions, emulsions, sedimentation*

## Introduction

Dispersions of liquid drops in an immiscible liquid are encountered in food, petroleum, cosmetics, paints, mineral, and chemical processing industries. The kinetics of creaming (or sedimentation) and coalescence of liquid drops are important to the phase separation stability of dispersions. Dispersions are shown,[1] in general, to consist of two zones: (1) a creaming or sedimentation zone in which drops are far apart from each other and (2) a densely packed zone in which the distance between adjacent drops is so small that they deform to form thin films of the intervening continuous phase. The latter zone forms when the volume rate of creaming (or sedimentation) is greater than that of the coalescence of drops with their bulk homophase at the coalescing interface (interfacial coalescence). This occurs when the Reynolds number of the creaming drops is high[1] or when the drops are stabilized by a surfactant

Present address of R. Hosig: Pizoler AG, Im Tiefriet, CH-7320 Sargans, Switzerland.
Correspondence concerning this article should be addressed to S. A. K. Jeelani at jeelani@ilw.agrl.ethz.ch.

or an additive, which inhibits droplet coalescence.[2] Lobo et al.[2] presented a model for the kinetic stability of creamed dense dispersions of small drops involving slight deformation and related the coalescence time of a single drop to the rate of increase in the mean drop size. In contrast, surfactant or additive free dispersions do not form a densely packed zone[3] when the creaming or sedimentation velocity of drops and thus the Reynolds number are extremely low, as would occur if either the drops are small or the density difference between the phases is small or the viscosity of the continuous phase is high. The present article aims at investigating such loosely packed but relatively concentrated creaming or sedimenting droplet dispersions, which is useful in understanding the interdrop and interfacial coalescence processes. Published experimental and theoretical information on such dispersions is not only limited but also restricted to dilute dispersions. For instance, Wang and Davis[3] experimentally investigated the temporal evolution of drop size distributions resulting from interdrop (binary) collisions and coalescence during sedimentation, and the kinetics of phase separation arising from interfacial coalescence. Unfortunately, only a few measurements on temporal evolution of drop size distributions were carried out at a single position in a dilute dispersion. The measured average drop diameter and interfacial coalescence rate increased initially with time as the result of interdrop collisions and coalescence, and subsequently decreased as larger drops sedimented out of the dispersion. These limited but important experimental results are useful to the present analysis.

Wang and Davis[3,4] extended and numerically solved the dynamic population balance model differential equations of Reddy et al.[5] to gravity-induced creaming of drops in a viscous flow regime and verified their experimental results on the phase separation kinetics. The drop volume concentration was 3.4% in the dispersion, which was sufficient for drop coalescence and phase separation to be investigated. They considered the dispersion to be dilute enough to validate their assumption of pairwise hydrodynamic interactions and van der Waals attraction between droplets to determine the efficiencies of collisions[6] due to gravity needed to compute the temporal evolutions of drop size distributions along the height of the dispersion. However, the Hamaker constant for the dispersion, needed to calculate the van der Waals attractive forces, was not known and so it was considered to be an adjustable model parameter. The value of this was obtained by fitting the numerical solutions of the population balance differential equations to the experimental data on the increase with time in the height of the coalesced drops with their bulk homophase.

Although the solutions of population balance equations require extensive numerical computations, they are based on first principles and provide significant information on the time-dependent drop size evolution. However, there is no literature on their application to concentrated creaming and coalescing dispersions, in which the droplet volume concentration is relatively high, as encountered in practical situations. This is attributed to the lack of fundamental quantitative information on the effect of neighboring drops on the pairwise interdrop gravitational collision rates and efficiencies in concentrated dispersions. This is further complicated by the inherent experimental difficulties associated with the measurement of the evolution of drop size distributions resulting from the relatively rapid coalescence during sampling in concentrated surfactant-free dispersions. Consequently, a simple model is developed herein, which characterizes the phase-separation stability of concentrated dispersions with respect to droplet creaming, and interdrop and interfacial coalescence. The model also enables the prediction of the temporal evolution of the average diameter of drops using the model parameters determined from the measured time-dependent heights of the coalescing and creaming interfaces.

It is clear from the above that only few studies have so far been carried out on surfactant or additive-free dispersions in which the Reynolds number of the creaming or sedimenting drops is very small. These are also limited to dilute dispersions and the existing theoretical analysis cannot be used for concentrated dispersions for the reasons mentioned above. The present article thus investigates experimentally concentrated rapeseed oil-in-water dispersions relevant to food emulsions in terms of the effect of the size distribution and concentration of drops on the kinetics of low Reynolds number creaming, drop size growth resulting from interdrop coalescence, and interfacial coalescence. The initial drop size distributions in dispersions are determined using a laser diffraction technique, whereas the time-dependent concentrations of creaming oil drops along the height of dispersion are recorded using a novel radioactive $\gamma$-ray density profile apparatus.[7] In addition, an analytical model is presented, which allows for the effects of concentration and growth in diameter of drops on creaming and coalescence. This describes well the present experimental results on concentrated dispersions and those of Wang and Davis[3] on dilute dispersions. The results obtained from the present model agree with those presented by Wang and Davis[3] using the population balance model. Furthermore, the present model enables the determination of the coalescence times of single drops with their bulk homophase at the coalescing interface using the experimental data on dispersions. These are in good agreement with those predicted by the theoretical equation[8,9] for drainage of the continuous phase film between the drop and its bulk homophase.

## Model

Consider a surfactant-free oil-in-water dispersion of initial height $h_0$ containing uniformly dispersed polydisperse oil drops of volume fraction $\varepsilon_0$, as shown in Figure 1. The lighter oil drops cream upward due to gravity, leaving a layer of clear heavier aqueous phase at the bottom. Because the drops have a size distribution, larger drops cream faster than the smaller drops, resulting in collisions and interdrop coalescence. Brownian collisions may also occur between very small drops. Drops arrive at the top coalescing interface and coalesce with the layer of clear bulk oil phase. When the volume rate of creaming is either equal to or lower than that of the interfacial coalescence, no zone of densely packed drops is formed below the coalescing interface because drops are far apart from each other and do not form continuous-phase films between them. This is explained by the fact that drops coalesce at the coalescing interface as soon as they arrive, without forming layers of drops one below the other. As discussed earlier, this would occur when the Reynolds number of creaming drops is extremely low if either the drops are small or the density difference between the phases is small or the viscosity of the continuous phase is high. However, drops initially undergo a larger

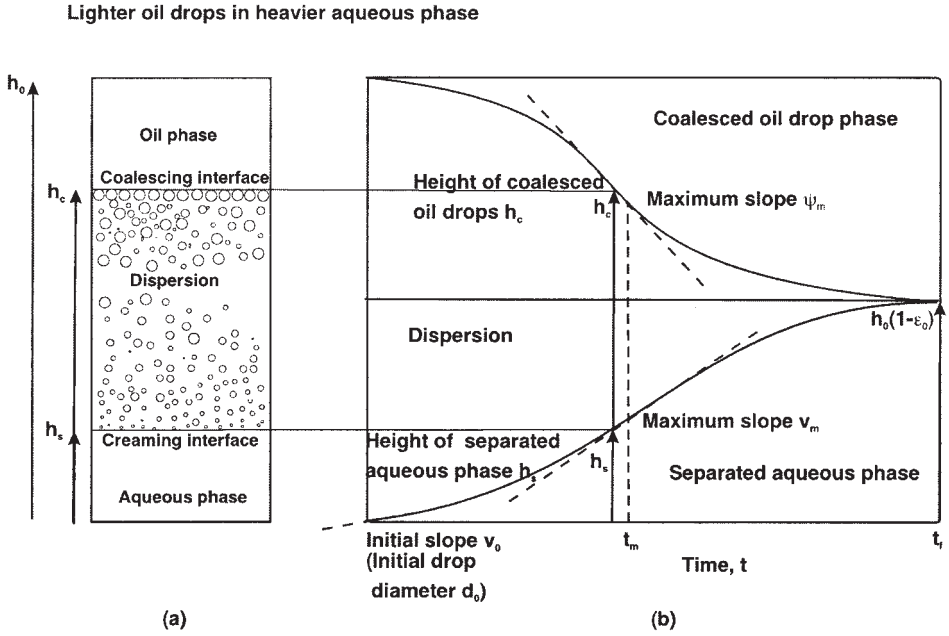


**Figure 1. (a) Simultaneous creaming and interfacial coalescence of oil drops in a dispersion; (b) typical variation with time $t$ in heights $h_s$ and $h_c$ of creaming and coalescing interfaces respectively.**

extent of binary coalescence because of differential creaming, resulting in an increase in the average drop diameter with time and a subsequent decrease because the bigger drops formed cream faster, leaving behind the smaller drops in the dispersion, as observed experimentally by Wang and Davis.[3] This would correspond to an increase in the velocity of the creaming interface with time initially followed by a decrease. For binary and interfacial coalescence, the drainage of the intervening continuous-phase film between two drops, and a drop and coalescing interface occurs; the film ruptures when its thickness is very small and van der Waals forces of attraction predominate.

### *Volume balance for dispersed and coalesced drops*

If $h_s$ and $h_c$ are the heights of the creaming and coalescing interfaces measured from the bottom of the vessel at any time $t$, then a volume balance for the oil phase gives

$$h_s\varepsilon = h_0(1 - \varepsilon_0) - h_c(1 - \varepsilon) \tag{1a}$$

in which the spatial average volume fraction of drops $\varepsilon$, in general, varies with time, its initial value being $\varepsilon_0$. This differentiates to give the volume flux balance

$$\{h_c - (1 - \varepsilon_0)h_0\}\frac{d\varepsilon}{dt} = \varepsilon^2 v - \varepsilon(1 - \varepsilon)\psi \tag{1b}$$

in which $v = dh_s/dt$ is the creaming velocity of drops relative to the vessel, and $\psi = -dh_c/dt$ is the volume rate of interfacial coalescence per unit area.

As drops cream upward, the height of the creaming interface $h_s$, which is identical with the height of the separated aqueous phase (see Figure 1b), increases with time $t$ from an initial value of zero to the final value of $h_s = h_0(1 - \varepsilon_0)$ when the dispersion separates into two clear phases in time $t_f$. In contrast, as the drops coalesce with their bulk homophase, the height of the coalescing interface $h_c$ decreases with time $t$ from an initial value of $h_0$ to the same final value as that of $h_s$ so that $h_c = h_s = h_0(1 - \varepsilon_0)$. The phase separation, characterized by the variations with time in the heights $h_s$ and $h_c$, depends on the creaming velocity and interfacial coalescence rate of drops. These are determined by the temporal evolution of the drop size distribution in the dispersion, which in turn is governed by interdrop collisions and coalescence as discussed below.

### *Temporal evolution of drop size distributions*

Wang and Davis[3] experimentally measured (filled squares in Figure 2) the temporal evolution of the average diameter of sedimenting propanediol drops in sebacic acid dibutylester at a height of 25 mm in a dilute, initially homogeneous, dispersion of height of 104 mm containing 3.4% by volume of drops of average diameter $d_0 = 28$ $\mu$m. Their results indicate that the average diameter $d$ of drops in the dispersion initially increases with time $t$ as a result of interdrop coalescence and subsequently decreases with time as larger drops formed sediment or cream out of dispersion, leaving behind smaller drops. Thus the average drop diameter attains its maximum value of $d_m$ in a time $t_m$ and reaches its final value of $d_f$ in a time $t_f$ when the dispersion separates into two phases. This observed temporal evolution of the average drop diameter $d$ in the dispersion is assumed in the present analysis to be given by the third-order polynomial in $t$

$$d = d_0\{c_0 + c_1 t + c_2 t^2 + c_3 t^3\} \tag{2}$$

This form of equation is assumed because it satisfies four criteria: (1) $d = d_0$ is the initial average drop diameter when

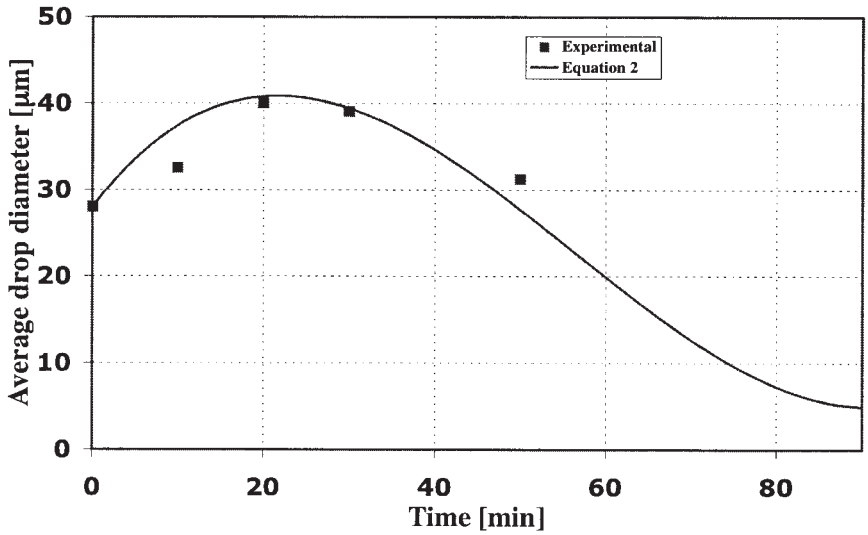


**Figure 2. Experimental (squares) evolution of average drop diameter at a height of 25 mm in a dispersion of initial total height of 104 mm containing 3.4% by volume of propanediol drops dispersed in sebacic acid dibutyl ester, observed by Wang and Davis.[3]**

The line represents the variation obtained using Eq. 2 by fitting the data.

$t = 0$; (2) $dd/dt = 0$ at time $t = t_m$ when the drops grow to their maximum diameter $d_m$; (3) the dispersion separates into two phases in time $t = t_f$ so that the final cut diameter $d = d_f$; and (4) $dd/dt = 0$ when $t = t_f$, to give the four constants: $c_0 = 1$, $c_1 = 6(1 - d_f/d_0)t_m/t_f(t_f - 3t_m)$, $c_2 = -3(1 - d_f/d_0)(t_m + t_f)/t_f^2(t_f - 3t_m)$, and $c_3 = 2(1 - d_f/d_0)/t_f^2(t_f - 3t_m)$. The final value of the average drop diameter $d_f$ corresponds to that below which interdrop collisions due to gravity become insignificant in comparison with the Brownian-induced collisions. This is encountered in a dispersion containing very small drops such as that used by Wang and Davis[3] shown in Figure 2. The initial rate of increase in the average drop diameter resulting from interdrop coalescence is given by $(dd/dt)_0 = d_0c_1$. The value of the maximum average drop diameter $d_m$ is obtained by setting $t = t_m$. For complete separation of the dispersion into two clear phases, $d_f = 0$ so that $c_1 = 6t_m/t_f(t_f - 3t_m)$, $c_2 = -3(t_m + t_f)/t_f^2(t_f - 3t_m)$, and $c_3 = 2/t_f^2(t_f - 3t_m)$. This is true for dispersions, which do not contain significant concentration of very small drops but involve relatively large drops as used in the present work.

Equation 2 can be used to describe the time-dependent variation in the average drop diameter at a given height within the dispersion using the corresponding local values of $t_m$ and $t_f$. The full line in Figure 2 represents the variation obtained by fitting the experimental data (filled squares) of Wang and Davis[3] to Eq. 2 using the values of $t_m = 21.67$ min and $t_f = 90.6$ min, the value of $d_f = 5$ $\mu$m being obtained as follows. As suggested by Zhang and Davis,[6] the value of the Peclet number $= \pi\Delta\rho g d_f^4\lambda(1 - \lambda^2)/24k\theta \gg 1$ for gravitational collisions to be more predominant than Brownian collisions between two drops of diameters $d$ and $d_f$ ($d < d_f$), where $\lambda = d/d_f$, $k = 1.381 \times 10^{-23}$ J/K is the Boltzmann constant, $\theta$ is the absolute temperature, $\Delta\rho$ is the density difference between the phases, and $g$ is the acceleration due to gravity. This occurs for values of about $d_f > 5$ $\mu$m for the dispersion shown in Figure 2 ($\Delta\rho = 99$ kg/m$^3$ and $\theta = 293$ K). However, because $d_f$ is the average diameter of drops, the polydisperse dispersion with a value of $d_f = 5$ $\mu$m would have a fraction of small drops with diameters $< 1$ $\mu$m. It can be seen that the experimental data are represented reasonably well by Eq. 2, the constants $c_1$, $c_2$, and $c_3$ being calculated using the above values of $t_m$, $t_f$, and $d_f$.

The temporal evolution of the average drop diameter in the dispersion depends on the extent of interdrop collisions and coalescence. This, in turn, is determined by the initial drop size distribution, polydispersity, concentration of drops, ratio of the viscosity of the drops to that of continuous phase, van der Waals forces of attraction, and hydrodynamic conditions, such as the residual turbulence in the dispersion. These factors affect the values of $t_m$ and $t_f$, which determine the values of the constants $c_1$, $c_2$, and $c_3$ in Eq. 2. Thus $t_m$ and $t_f$ can be obtained directly from the experimental data on temporal evolution of the average drop diameter in the dispersion. However, as explained later in the Experimental section, problems associated with rapidly coalescing large drops during sampling and measurement make it difficult to determine accurately the experimental evolution of drop size distributions in surfactant-free concentrated dispersions. Alternatively, the values of $t_m$ and $t_f$ can be obtained from the measured variations with time $t$ in the heights $h_c$ and $h_s$ of the coalescing and creaming interfaces as follows.

Irrespective of whether visual, optical, or radioactive $\gamma$-ray density profile apparatus or other method used to measure the positions of the creaming and coalescing interfaces, $t_f$ can be determined experimentally with reasonable accuracy using the volume balance; that is, the final heights of the coalescing and creaming interfaces $h_c$ and $h_s$ must both be equal to $h_0(1 - \varepsilon_0)$ when complete separation of a surfactant-free dispersion into two clear phases occurs. This is true for dispersions in which the drops are relatively large, as in the present work. Knowing $t_f$, one can calculate $t_m$ because these are interrelated by Eq. 10b, as shown later. In contrast, for dispersions involving small drops, as used in the work of Wang and Davis,[3] primary

separation is complete in time $t_f$ when the separated aqueous phase contains very small drops of average diameter $d_f$, below which gravitational creaming is negligible. The latter is indicated by the fact that the positions of the interfaces remain virtually constant with respect to time but the final volume balance is not fully satisfied. However, in the present work, the constants $c_1$, $c_2$, and $c_3$ are determined using the values of $t_f$ (also $t_m$ for the results of Wang and Davis[3]) obtained by fitting the experimental variations with time $t$ in the heights $h_c$ and $h_s$ of the coalescing and creaming interfaces to those described by the model Eqs. 9 and 8, respectively, derived later. These are then used to predict the temporal evolution of the average diameter of drops in the dispersion using Eq. 2. The effect of interdrop coalescence on creaming, interfacial coalescence, and phase separation in dispersions is discussed below.

### *Creaming velocity and interfacial coalescence rate*

The creaming velocity of drops of average diameter $d$ relative to the vessel in a batch dispersion for the viscous flow regime [Reynolds number $\rho_c dv/\mu_c(1-\varepsilon) \ll 10$], is given[1] by

$$v = \frac{dh_s}{dt} = \frac{\Delta\rho g d^2(1-\varepsilon)^2}{18\mu_c(1+4.56\varepsilon)} \tag{3a}$$

in which $\Delta\rho$ is the density difference between the phases; $\mu_c$ and $\rho_c$ are the continuous phase viscosity and density, respectively; and $g$ is the acceleration due to gravity. The spatial average volume fraction of drops $\varepsilon$ will not significantly change with time, so that $\varepsilon = \varepsilon_0$ when the volume rate of interfacial coalescence is either equal to or greater than the volume rate of creaming as occurs in surfactant-free and low-density difference fast-coalescing systems. This was also implicitly assumed by Wang and Davis[3] in their analysis. Equation 3a would then become

$$v = \frac{dh_s}{dt} = v_0\left(\frac{d}{d_0}\right)^2 \tag{3b}$$

in which

$$v_0 = \frac{\Delta\rho g d_0^2(1-\varepsilon_0)^2}{18\mu_c(1+4.56\varepsilon_0)} \tag{3c}$$

is the initial creaming velocity. The volume and volume flux balance Eqs. 1a and 1b then reduce to

$$h_s\varepsilon_0 = (h_0 - h_c)(1-\varepsilon_0) \tag{4a}$$

$$\varepsilon_0 v = (1-\varepsilon_0)\psi \tag{4b}$$

The volume rate of interfacial coalescence of drops per unit area $\psi$ is given from Eqs. 4b and 3b for volume flux balance and creaming velocity as

$$\psi = -\frac{dh_c}{dt} = \psi_0\left(\frac{d}{d_0}\right)^2 \tag{5a}$$

in which

$$\psi_0 = \frac{\varepsilon_0 v_0}{(1-\varepsilon_0)} \tag{5b}$$

is the initial interfacial coalescence rate for drops of diameter $d_0$. Because the time-dependent average drop diameter varies according to Eq. 2, both the creaming velocity $v$ and specific interfacial coalescence rate $\psi$ increase with time until their maximum values ($v_m$ and $\psi_m$) are reached at $t_m$, corresponding to the maximum average drop diameter $d_m$, and decrease thereafter until they become equal to zero at time $t_f$ when dispersion separates into two clear phases.

The volume rate of interfacial coalescence per unit area is shown[10] to be given by

$$\psi = \frac{2d\varepsilon}{3\tau} \tag{6}$$

in which $\tau$ is the coalescence time of drops of diameter $d$ and volume fraction $\varepsilon = \varepsilon_0$ at the coalescing interface. Equating the two values of $\psi$, given by Eqs. 5a and 6, gives the hyberbolic decrease in interfacial coalescence time with average drop diameter

$$\tau = \tau_0\left(\frac{d_0}{d}\right) \tag{7a}$$

in which the interfacial coalescence time $\tau_0$ of drops of diameter $d_0$ and volume fraction (hold-up) $\varepsilon_0$ is given by

$$\tau_0 = \frac{12\mu_c(1+4.56\varepsilon_0)}{\Delta\rho g d_0(1-\varepsilon_0)} \tag{7b}$$

### *Volumes of separated continuous phase and coalesced drops*

Substituting for the variation in the average drop diameter with time given by Eq. 2 and integrating Eq. 3b with the initial condition $h_s = 0$ when $t = 0$ gives the time-dependent variation in height $h_s$ of the separated continuous aqueous phase (or creaming interface)

$$h_s = v_0 t\{1 + k_1 t + k_2 t^2 + k_3 t^3 + k_4 t^4 + k_5 t^5 + k_6 t^6\} \tag{8}$$

in which $k_1 = c_1$, $k_2 = (2c_2 + c_1^2)/3$, $k_3 = (c_3 + c_1 c_2)/2$, $k_4 = (2c_1 c_3 + c_2^2)/5$, $k_5 = c_2 c_3/3$, and $k_6 = c_3^2/7$.

The time-dependent variation in the height of the coalescing interface can then be obtained from the volume balance Eq. 4a as

$$h_c = h_0 - \frac{\varepsilon_0 v_0 t}{(1-\varepsilon_0)} \times \{1 + k_1 t + k_2 t^2 + k_3 t^3 + k_4 t^4 + k_5 t^5 + k_6 t^6\} \tag{9}$$

which can also be obtained by integrating the volume flux Eq. 5a with the initial condition $h_c = h_0$ when $t = 0$.

As explained earlier, the creaming velocity $v = dh_s/dt$ and interfacial coalescence rate $\psi = -dh_c/dt$ attain their maximum values of $v_m$ and $\psi_m$, respectively, at time $t_m$ when drops grow to their maximum average diameter $d_m$. This results in an inflection point in the variations with time in the heights $h_s$ and $h_c$ of the creaming and coalescing interfaces given by Eqs. 8 and 9 at time $t_m$ where the slopes are maximum.

When all the drops have coalesced with their bulk homophase at time $t_f$, corresponding to complete separation of the dispersion, into two clear phases so that $d_f = 0$ and $h_s = h_0(1 - \varepsilon_0)$, Eq. 8 reduces to the quadratic equation in $T_m = v_0 t_m / h_0(1 - \varepsilon_0)$ as

$$AT_m^2 + BT_m + C = 0 \tag{10a}$$

where $A = 63(5 - T_f)$, $B = 14T_f(4T_f - 15)$, $C = T_f^2(35 - 13T_f)$, and $T_f = v_0 t_f / h_0(1 - \varepsilon_0)$. The roots of this equation are given by

$$T_m = \frac{B}{2A}\left[-1 \pm \sqrt{1 - \frac{4AC}{B^2}}\right] \tag{10b}$$

which enable the determination of $t_m$ if $t_f$ is known experimentally for a given dispersion of initial height $h_0$, dispersed phase volume fraction $\varepsilon_0$, and average drop diameter $d_0$ because the initial creaming velocity can be found using Eq. 3c. The maximum drop diameter $D_m = d_m/d_0$, attributed to interdrop coalescence, can then be obtained from Eq. 2 as

$$D_m = \frac{d_m}{d_0} = \frac{(T_f - T_m)^3}{T_f^2(T_f - 3T_m)} \tag{11}$$

in which $T_m$ is given by Eq. 10b, which in turn is determined by $T_f$.

## Experimental

### *Liquid–liquid system*

The dispersed and continuous phases are rapeseed oil and demineralized water (boiled to remove dissolved gases). The viscosity of rapeseed oil, measured using a DSR rheometer (Rheometric Scientific, Piscataway, NJ), was 56.5 mPa·s at 25°C; the density, measured using a density meter (Anton Paar, Graz, Austria), was 914 kg/m$^3$. The corresponding values for water were 1 mPa·s and 997 kg/m$^3$. The interfacial tensions measured by the drop volume method for unequilibrated and equilibrated phases were 21.36 and 21.45 mN/m at 25°C, indicating that the mutual solubilities of the aqueous and organic phases are negligible.

### *Mixing unit and phase separation cell*

The mixing unit for the formation of dispersions is a 1-L double-walled glass vessel (115 mm diameter) with an outer jacket for circulating water from a thermostat to regulate the temperature. The Polytron (Kinematica AG, Littau-Lucerne, Switzerland) high shear stainless steel concentric stator/rotor impeller consists of an outer stator (depth: 22 mm; OD: 35 mm; ID: 29 mm) and an inner rotor (width: 8 mm; OD: 27 mm; ID: 20 mm), with speed adjustable up to several thousand rpm. A 360-mm-tall transparent cell of rectangular cross section (40 × 66 mm) made of 2-mm-thick polycarbonate plates is used for the creaming, coalescence, and phase separation studies of the droplet dispersions.

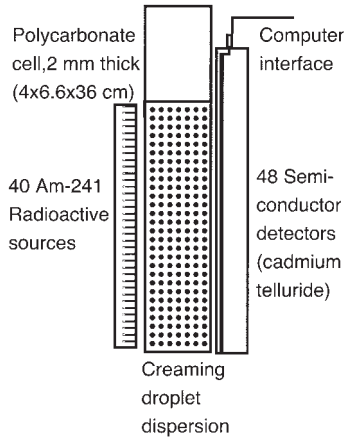


**Figure 3. γ-Ray density profile apparatus showing the polycarbonate cell for the dispersion sandwiched between the vertical array of radioactive sources and semiconductor detectors.**

### *γ-Ray density profile apparatus*

The γ-ray density profile apparatus (GDPA) developed at our institute in collaboration with Eurorad (Strasbourg, France) is described in detail elsewhere,[7,11] but is described briefly here for the sake of better understanding. This works on the principle that the intensity $I$ of attenuated γ-ray photons depends on the path length, density of liquid, and mass absorption coefficient. The latter does not vary significantly for organic liquids, and is about the same as that for water. Thus $I$ depends only on the average density of a dispersion, which is a function of the densities of drop and continuous phases, and their volume concentrations.

The GDPA consists of a vertical array of 40 americium-241 radioactive sources (6 mm apart) mounted on a vertical rod opposite to which 48 cadmium telluride semiconductor detector cells (5.3 mm high) are vertically stacked, one above the other, as shown in Figure 3. The polycarbonate settler cell can be introduced between the sources and detectors, which can be cooled by a cryostat if necessary. The electric outputs from the detectors are amplified and processed by a personal computer (PC) to give the time-dependent variation in the volume (hold-up) fraction of oil drops or water along the height of the settler cell. The isotope americium-241 has a half-life of 457.7 years and decays emitting γ-ray photons predominantly with energies of 59.5 keV, of which the radiation intensity is 1 million photons s$^{-1}$ steradian$^{-1}$ for every source. For safety reasons, the source holder is embedded in a sliding lead door while the detector holder is held between three sealed lead plates.

When γ-rays of intensity $I_0$ photons/s pass through a liquid of density $\rho$ and thickness $L$, they become attenuated to an intensity of $I$ photons/s given by the Lambert–Beers law

$$I = I_0 e^{-\rho L \alpha} \tag{12a}$$

in which the mass absorption coefficient $\alpha$ depends on the energy of the $\gamma$-rays and the atomic number of liquid. Depending on the energy, $\gamma$-rays attenuate by interacting with matter as a result of photoelectric, Compton, and pair production effects. For low atomic number liquids and relatively low energy $\gamma$-radiation, as in the present case, the Compton effect is predominant. The value of $\alpha$ is usually small, so that $\alpha\rho L \ll 1$ and

$$I = I_0(1 - \rho L\alpha) \tag{12b}$$

in which $\alpha$ is constant for a given liquid or dispersion.

A semiconductor detector works on the principle that, under the influence of an applied voltage, it generates a short electrical pulse when a $\gamma$-ray photon hits it. The pulse is amplified and the signal is stored in the PC. Thus the number $N$ of pulses in unit time gives the intensity of the $\gamma$-ray photons transmitted through a liquid of density $\rho$ in the polycarbonate cell, so that Eq. 12b can be written as

$$\rho = c - mN \tag{13a}$$

The values of the slope $m = 1/N_0L\alpha$ and intercept $c = 1/L\alpha$ can be determined by using the values of the number of pulses measured in a given time interval by the detectors of the GDPA for two different liquids of known densities. Equation 13a can then be used to determine the density of an oil-in-water (or water-in-oil) dispersion by measuring the number of pulses $N$ in the same time interval as follows. The average density $\rho$ of a dispersion containing an aqueous phase of density $\rho_w$ and volume fraction $\varepsilon_w$, and an organic phase of density $\rho_o$ and volume fraction $\varepsilon_o = 1 - \varepsilon_w$ can be written as

$$\rho = \rho_w\varepsilon_w + \rho_o(1 - \varepsilon_w) \tag{13b}$$

which, when combined with Eq. 13a, gives

$$\varepsilon_w = \frac{(c - \rho_o - mN)}{(\rho_w - \rho_o)} \tag{13c}$$

The values of $m = 0.00544$ kg sm$^{-3}$, $c = 2237$ kg/m$^3$, and a regression coefficient close to unity are obtained by fitting the number of pulses measured in 30 s by the detectors of the GDPA using Eq. 13a for three different liquids: *n*-heptane, isooctane, and demineralized water, with densities of 681, 693, and 997 kg/m$^3$, respectively. Panoussopoulos,[7] who described the details of the methods of calibration and measurement, also demonstrated that this method is not only reasonably accurate but also can be used for opaque liquid systems.

### *Procedure*

In a typical experiment, rapeseed oil drops in water dispersion is formed by filling the mixing vessel with water and positioning the impeller at the bottom to prevent air entrapment. The motor is switched on, the impeller speed set at desired value, and rapeseed oil added slowly (about 8 L/h) through a 1-mm-diameter Teflon tube immersed in water, close to the suction area of the rotor using a peristaltic pump. As the level of dispersion increases, the impeller position is raised until all oil is added to give the desired oil volume fraction. Then the impeller is raised to the middle of the dispersion and agitation continued until the end of the desired mixing time (10 min). The temperature of dispersion is maintained at the desired value (24.5°C) using the controller on the thermostat arrangement. The motor is then switched off and the dispersion is transferred into the phase separation (settler) cell, which is placed in the GDPA. The data-acquisition software Eurosca3 (supplied by Eurorad) on the PC is activated to record the number of $\gamma$-photons (counts in a small time interval) hitting the detectors as a function of time until the dispersion separates into two phases. These stored digital scans are then processed using the software ETHscan, developed at our institute to obtain the variation in the volume fraction (hold-up) of oil drops along the height of the settler cell. For comparison purposes, the rapeseed oil-in-water dispersion, formed once again under identical operating conditions, is poured into the settler cell and the variations with time in the positions of the creaming and coalescing interfaces are recorded visually. To measure the drop size distribution using Malvern laser diffraction method, 4 mL of dispersion immediately after its formation is stabilized by the addition of 50 mL demineralized water containing 5 wt % of sodium dodecyl sulfate (much greater than the critical micelle concentration). The procedure is repeated by forming dispersions at different agitation speeds and volume fractions of rapeseed oil drops, listed in Table 1.

Wang and Davis[3] measured the temporal evolution of drop size distributions in dilute ($\varepsilon_0 = 0.034$) dispersions containing small drops ($d_0 = 28$ $\mu$m) by drawing a sample with a syringe and analyzing it under a microscope. They chose the size of the syringe to minimize coalescence of drops during sampling. However, as discussed earlier, they carried out only very few measurements, which were restricted to a single position in the dispersion, as shown (filled squares) in Figure 2. They also attempted to measure the drop size distributions *in situ* using video microscopy because both the drops and the continuous phase were transparent and the images of drops in front did not completely obscure those in the focal plane behind. They concluded that the *in situ* results agreed only qualitatively with those determined using the off-line sampling technique. Their work demonstrates the difficulties involved in measuring the temporal evolution of drop size distributions even in dilute dispersions.

The problem of coalescence and creaming of drops during sampling and measurement is far greater in concentrated ($\varepsilon_0 \geq 0.3$) surfactant-free dispersions containing rapidly coalescing and relatively large drops used in the present work. This could, in principle, be overcome by drawing drops from the dispersion using a syringe containing a stabilizer solution such that drops entering the syringe could be immediately stabilized. However, the accuracy of the method needs to be tested. Consequently, as described earlier, Eq. 2 can be used to predict the temporal evolution of the average drop diameter in the dispersion, whose constants $c_1$, $c_2$, and $c_3$ are determined using the values of $t_f$ obtained by fitting the experimental variations with time $t$ in the heights $h_c$ and $h_s$ of the coalescing and creaming interfaces to the model Eqs. 9 and 8, respectively.

Table 1. Experimental Values of Initial Conditions $\varepsilon_0$, $d_0$, $h_0$, and Model Parameters for the Present and Published Results

| Parameter | Experiment | | | | | | | |
|---|---|---|---|---|---|---|---|---|
| | 1a | 1b | 2a | 2b | 3a | 3b | Wang and Davis (1996) | |
| Speed, rpm | 1500 | 2200 | 1500 | 2200 | 1500 | 2200 | — | — |
| $\varepsilon_0$ | 0.291 | 0.298 | 0.394 | 0.393 | 0.504 | 0.501 | 0.034 | 0.034 |
| $h_0$, mm | 285 | 282 | 282 | 283 | 283 | 283.5 | 100 | 145 |
| $d_0$, $\mu$m | 70 | 55 | 146 | 105 | 270 | 200 | 28 | 28 |
| $t_m$, min | 6.5 | 10.7 | 2.2 | 2.9 | 1.13 | 1.45 | 27.2 | 20 |
| $t_f$, min | 22.674 | 37.33 | 7.724 | 9.802 | 4.079 | 5.014 | 90.6 | 64.3 |
| $v_0$, mm/min | 2.87 | 1.72 | 7.59 | 3.94 | 14.76 | 8.35 | 0.23 | 0.23 |
| $\psi_0$, mm/min | 1.18 | 0.73 | 4.93 | 2.55 | 14.97 | 8.38 | 0.008 | 0.008 |
| $(dd/dt)_0$, $\mu$m/min | 38 | 18 | 222 | 169 | 652 | 523 | 4.6 | 10 |
| $\mathrm{Re}_0$ | 0.0047 | 0.0022 | 0.0304 | 0.0113 | 0.1334 | 0.0556 | $10^{-5}$ | $10^{-5}$ |
| $d_m$, $\mu$m | 182 | 143 | 367 | 327 | 604 | 543 | 84.3 | 117.5 |
| $v_m$, mm/min | 19.3 | 11.5 | 48.0 | 38.0 | 73.9 | 61.4 | 2.1 | 4.0 |
| $\psi_m$, mm/min | 7.9 | 4.9 | 31.1 | 24.6 | 75.0 | 61.6 | 0.07 | 0.14 |
| Measured $\tau_0$, ms | 691 | 901 | 467 | 647 | 363 | 478 | 4749 | 4749 |
| Predicted $\tau_0$, ms | 875.3 | 1176.9 | 530.4 | 774.9 | 369.0 | 514.5 | 2741.1 | 2741.1 |
| $Ca\left(\frac{\delta_i}{2d_0}\right)^2 \times 10^{11}$ | 1.83 | 1.77 | 1.11 | 1.11 | 0.63 | 0.65 | 44.7 | 44.7 |
| $f \times 10^{11}$, N | 4.46 | 2.11 | 28.71 | 10.71 | 126.1 | 52.56 | 0.934 | 0.934 |

## Results and Discussion

### *Present work*

The experimental drop size distributions measured using a laser diffraction technique in rapeseed oil dispersed in water dispersion formed in the mixer at two agitation speeds (1500 and 2200 rpm) and two volume fractions of rapeseed oil drops ($\varepsilon_0 = 0.3$ and 0.4 nominally) are shown in Figure 4. When the initial oil drop volume fraction is about 0.3, the drop size distribution shifts toward the lower sizes, and the volume-surface (Sauter) mean drop diameter $d_0$, listed in Table 1, decreases from 70 to 55 $\mu$m (standard deviations being 22 and 19 $\mu$m, respectively) as the agitation speed is increased from 1500 to 2200 rpm. An increase in the initial drop volume fraction to 0.4 in the dispersion increases the value of $d_0$ by almost a factor of 2 (146 $\mu$m at 1500 rpm and 105 $\mu$m at 2200 rpm with standard deviations of 17 and 19 $\mu$m, respectively). The values of $d_0$ for $\varepsilon_0 = 0.5$ listed in Table 1 are obtained by fitting the phase-separation data to the model, given that they could not be accurately measured because of creaming of large drops in the measuring cell of the Malvern laser diffraction instrument.

A typical time-dependent variation in the volume fraction of water along the height of a rapeseed oil-in-water dispersion, measured using the GDPA during creaming, coalescence, and phase separation, is shown in Figure 5 when the initial volume fraction and average diameter of oil drops are, respectively, $\varepsilon_0$

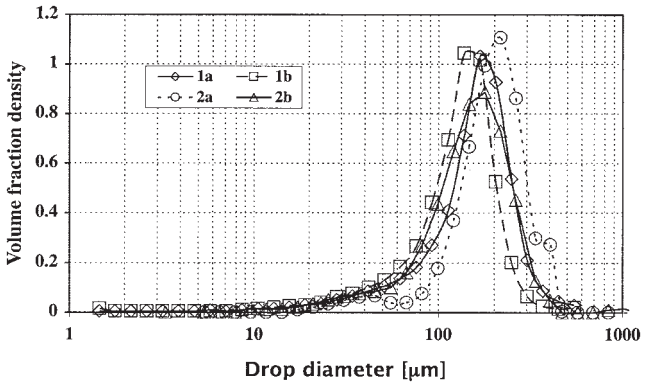


**Figure 4. Experimental initial size distributions of rapeseed oil drops in water dispersions formed in a mixer under different agitation speeds and nominal dispersed phase concentrations.**

1a: $\varepsilon_0 = 0.291$, 1500 rpm; 1b: $\varepsilon_0 = 0.298$, 2200 rpm; 2a: $\varepsilon_0 = 0.394$, 1500 rpm; 2b: $\varepsilon_0 = 0.393$, 2200 rpm.

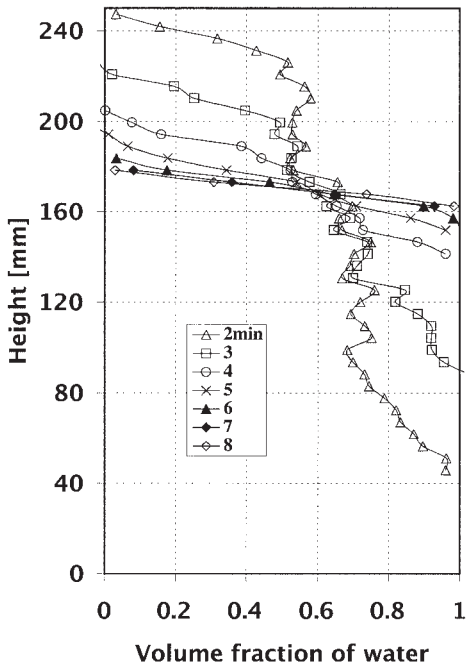


**Figure 5. Time-dependent variation in volume fraction of water along the height of dispersion measured using GDPA for an initial volume fraction of oil drops $\varepsilon_0 = 0.393$, and average drop diameter $d_0 = 105$ $\mu$m.**

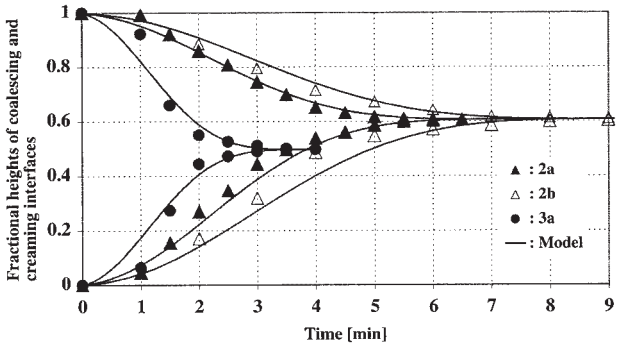


**Figure 6. Comparison between experimental (symbols) and theoretical (lines) variations with time in fractional heights of coalescing $h_c/h_0$ (upper) and creaming $h_s/h_0$ (lower) interfaces during separation of dispersions with different initial conditions.**

2a: $\varepsilon_0 = 0.394$, $d_0 = 146$ $\mu$m; 2b: $\varepsilon_0 = 0.393$, $d_0 = 105$ $\mu$m; 3a: $\varepsilon_0 = 0.504$, $d_0 = 270$ $\mu$m.

$= 0.393$ and $d_0 = 105$ $\mu$m (see Table 1). For a given time, the point of intersection of a curve with the vertical axis, where the volume fraction of water is 0 (upper region on left), gives the position of the coalescing interface where oil drops coalesce to form a layer of bulk homophase. Similarly the point of intersection of a curve with the vertical axis, where the volume fraction of water is 1 (lower region on right), yields the position of the creaming interface below which a layer of separated water has formed. Thus the volume fraction of water can be seen to decrease from a value of 1 at the bottom to a value of 0 at the top of the dispersion corresponding to an increase in the volume fraction of rapeseed oil drops from 0 to 1. The instantaneous sum of volumes of water separated as a result of creaming and that present in the dispersion as continuous phase (which is the area under each of the curves) must be equal to the volume of water initially present in the dispersion

$$h_s + \int_{h_s}^{h_C} (1 - \varepsilon) dz = (1 - \varepsilon_0) h_0 \qquad (14)$$

This is used to determine the time-dependent positions $h_s$ and $h_c$ of the creaming and coalescing interfaces from the GDPA results until the dispersion separated into two phases for all the experiments listed in Table 1. The error between the experimental initial volume fraction of water and that obtained using the above integral by linear approximations for the profiles measured by GDPA is less than about 2.5% for most of the data. Figure 5 shows that a layer of closely packed drops forms at the top of the dispersion, especially during the initial period, as indicated by the height over which the volume concentration of oil drops is $>0.75$ (volume fraction of water is $<0.25$), corresponding to monodispersed spheres. However, the thickness of this layer is small compared with the total height of the dispersion so that the dispersion is essentially loosely packed during most of the time period.

Figures 6 and 7, respectively, show the experimental (symbols) variations with time in the fractional heights of coalescing $h_c/h_0$ (upper) and creaming $h_s/h_0$ (lower) interfaces measured during the droplet creaming and coalescence in the dispersions with different initial volume fractions $\varepsilon_0$ and average diameters $d_0$ of drops. The dispersions separated completely into two clear phases, as indicated by the fact that the final values of the fractional heights of the coalescing and creaming interfaces are equal to $(1 - \varepsilon_0)$. This is because the dispersion initially contained mainly relatively large drops (see Figure 4 for negligible concentration of small drops of diameter $< 10$ $\mu$m), which underwent gravitational collisions (the Peclet number is very much larger than unity) and creaming leading to its complete separation ($d_f = 0$). As discussed under Eq. 2, the constants in model Eqs. 9 and 8, for the prediction of the heights of the coalescing and creaming interfaces, are then given by $c_1 = 6t_m/t_f(t_f - 3t_m)$, $c_2 = -3(t_m + t_f)/t_f^2(t_f - 3t_m)$, and $c_3 = 2/t_f^2(t_f - 3t_m)$, in which $t_m$ is related to $t_f$ by Eq. 10b.

In principle, the measured separation time $t_f$ of the dispersion can be used to obtain the constants $c_1$, $c_2$, and $c_3$. However, to minimize inaccuracies, the value of $t_f$ is obtained by fitting the experimental data in Figures 6 and 7 to Eqs. 9 and 8, respectively. The time-dependent variations in $h_c/h_0$ and $h_s/h_0$ so obtained using these equations are shown by the full lines in the figures. In general, the agreement between the experimental and theoretical results is good in spite of the simplicity of the model. It is evident that the larger the values of initial concentration $\varepsilon_0$ and average diameter of the drops $d_0$ are, the shorter the times needed for the drops to cream and coalesce from the dispersion, thereby separating into two phases. The heights of the creaming interface for low and high initial oil drop volume fractions at high agitation speeds could not be accurately determined from the GDPA, given that the creaming interface is not sharp because of very fine secondary droplets. Consequently, these could not be shown in Figure 7. The experimental values of the initial average drop diameter $d_0$, drop volume fraction $\varepsilon_0$, and dispersion height $h_0$, together with the fitted values of the model parameter $t_f$ and calculated values of $t_m$ using Eq. 10b, are listed in Table 1. The values of the initial creaming velocity $v_0$, interfacial coalescence rate $\psi_0$, rate of increase in drop diameter $(dd/dt)_0$, and interfacial coalescence

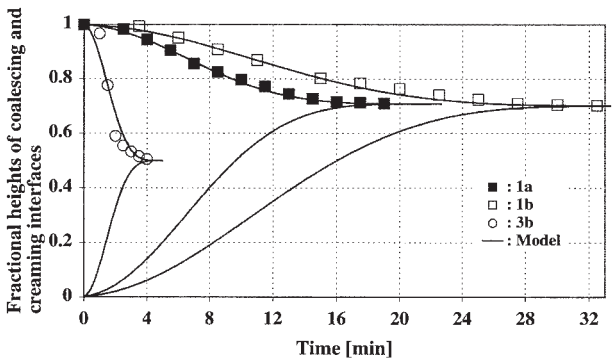


**Figure 7. Comparison between experimental (symbols) and theoretical (lines) variations with time in fractional heights of coalescing $h_c/h_0$ (upper) and creaming $h_s/h_0$ (lower) interfaces during separation of dispersions with different initial conditions.**

1a: $\varepsilon_0 = 0.291$, $d_0 = 70$ $\mu$m; 1b: $\varepsilon_0 = 0.298$, $d_0 = 55$ $\mu$m; 3b: $\varepsilon_0 = 0.501$, $d_0 = 200$ $\mu$m.

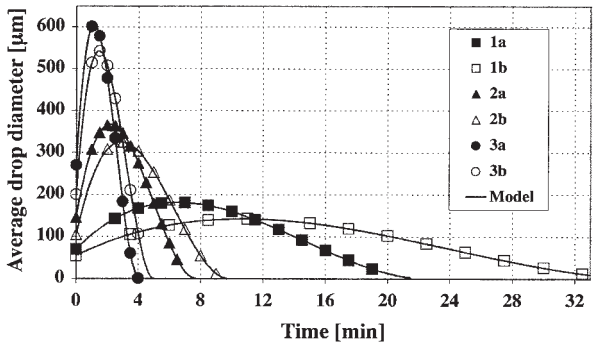


**Figure 8. Predicted (lines) variation with time in average drop diameter during droplet creaming in dispersions with different initial conditions.**

1a: $\varepsilon_0 = 0.291$, $d_0 = 70$ $\mu$m; 1b: $\varepsilon_0 = 0.298$, $d_0 = 55$ $\mu$m; 2a: $\varepsilon_0 = 0.394$, $d_0 = 146$ $\mu$m; 2b: $\varepsilon_0 = 0.393$, $d_0 = 105$ $\mu$m; 3a: $\varepsilon_0 = 0.504$, $d_0 = 270$ $\mu$m; 3b: $\varepsilon_0 = 0.501$, $d_0 = 200$ $\mu$m. The symbols represent the theoretical values corresponding to the experimental data in Figures 6 and 7.

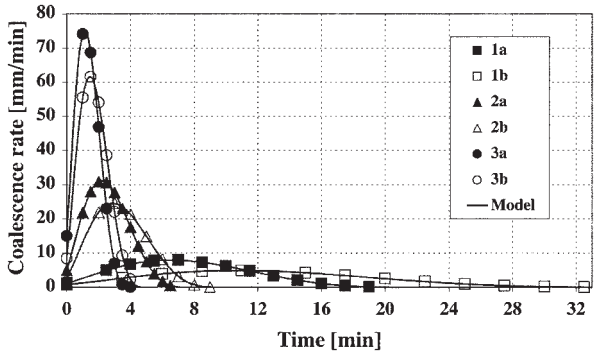


**Figure 10. Predicted (lines) variation with time in droplet coalescence rate in dispersions with different initial conditions.**

1a: $\varepsilon_0 = 0.291$, $d_0 = 70$ $\mu$m; 1b: $\varepsilon_0 = 0.298$, $d_0 = 55$ $\mu$m; 2a: $\varepsilon_0 = 0.394$, $d_0 = 146$ $\mu$m; 2b: $\varepsilon_0 = 0.393$, $d_0 = 105$ $\mu$m; 3a: $\varepsilon_0 = 0.504$, $d_0 = 270$ $\mu$m; 3b: $\varepsilon_0 = 0.501$, $d_0 = 200$ $\mu$m. The symbols represent the theoretical values corresponding to the experimental data in Figures 6 and 7.

time $\tau_0$ for drops of diameter $d_0$ determined using Eqs. 3c, 5b, 2, and 7b, respectively, are also tabulated.

Figures 8, 9, and 10, respectively, show the time-dependent average drop diameter $d$, creaming velocity $v$, and interfacial coalescence rate $\psi$, predicted by model Eqs. 2, 3b, and 5a corresponding to the data shown in Figures 6 and 7. The symbols also refer to predicted values but correspond to the specific experimental times. It can be seen that the average drop diameter increases initially with time as a result of interdrop coalescence until a maximum value is reached, and subsequently decreases as larger drops cream out of the dispersion. Consequently, the corresponding creaming velocity $v$ and interfacial coalescence rate $\psi$ increase initially until their maximum values are attained and decrease thereafter. This is consistent not only with the present experimental observations but also with those of Wang and Davis.[3] It is clear from Table 1 that the larger the initial drop diameter $d_0$ and drop volume fraction $\varepsilon_0$ are, the larger are the values of the initial rate of increase in the average drop diameter $(dd/dt)_0$, and the maximum values of the average drop diameter $d_m$, creaming velocity $v_m$, and interfacial coalescence rate $\psi_m$, and the shorter are the corresponding time $t_m$ and time of completion of creaming and coalescence $t_f$.

Concentrated dispersions, which have larger initial average drop diameter $d_0$, result in faster initial creaming velocity $v_0$ and interfacial coalescence rate $\psi_0$. For instance, for the dispersions formed in a mixer at an agitation speed of 1500 rpm, Table 1 indicates that as $d_0$ increases from 70 to 270 $\mu$m corresponding to an increase in $\varepsilon_0$ from 0.3 to 0.5, $v_0$ increases from 2.9 to 14.8 mm/min because of an increase in $(dd/dt)_0$ from 38 to 652 $\mu$m/min. Consequently, $\psi_0$ increases from 1.2 to 15 mm/min, resulting in a decrease in $t_f$ from 22.7 to 4.1 min. The corresponding decrease in the initial interfacial coalescence time $\tau_0$ is from 691 to 363 ms. An increase in the agitation speed in the mixer to 2200 rpm decreases the values of $d_0$, $v_0$, $(dd/dt)_0$, and $\psi_0$, and increases $t_f$. The Reynolds number $\mathrm{Re}_0 \ll 1$, indicating that droplet creaming corresponds to viscous flow regime as assumed in the analysis.

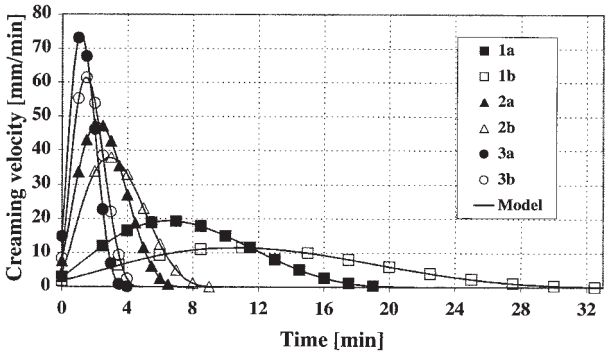


**Figure 9. Predicted (lines) variation with time in droplet creaming velocity in dispersions with different initial conditions.**

1a: $\varepsilon_0 = 0.291$, $d_0 = 70$ $\mu$m; 1b: $\varepsilon_0 = 0.298$, $d_0 = 55$ $\mu$m; 2a: $\varepsilon_0 = 0.394$, $d_0 = 146$ $\mu$m; 2b: $\varepsilon_0 = 0.393$, $d_0 = 105$ $\mu$m; 3a: $\varepsilon_0 = 0.504$, $d_0 = 270$ $\mu$m; 3b: $\varepsilon_0 = 0.501$, $d_0 = 200$ $\mu$m. The symbols represent the theoretical values corresponding to the experimental data in Figures 6 and 7.

### *Comparison with other published experimental data and models*

The present model is compared with the drop population balance model and experimental results of Wang and Davis[3] on dilute dispersions involving the sedimentation and coalescence of heavier (1037 kg/m$^3$) and viscous (56 mPa·s) propanediol drops dispersed in lighter (938 kg/m$^3$) and viscous (9 mPa·s) sebacic acid dibutyl ester. Figure 11 shows their experimental (circles) variation with time in % volume of drops coalesced with bulk homophase for a dilute dispersion ($\varepsilon_0 = 0.034$) of initial height 145 mm (see Table 1 for initial conditions). The full line represents the variation described by the present model using experimental value of initial average drop diameter $d_0$ and the values of the model parameters $t_m$ and $t_f$ (listed in Table 1) obtained by fitting the experimental data to Eq. 9. As discussed earlier, a value of $d_f = 5$ $\mu$m is assumed, given that the Peclet number $\gg 1$ for drops larger than this diameter, so that gravitational collisions are more important than Brownian collisions. The dashed line represents the variation presented

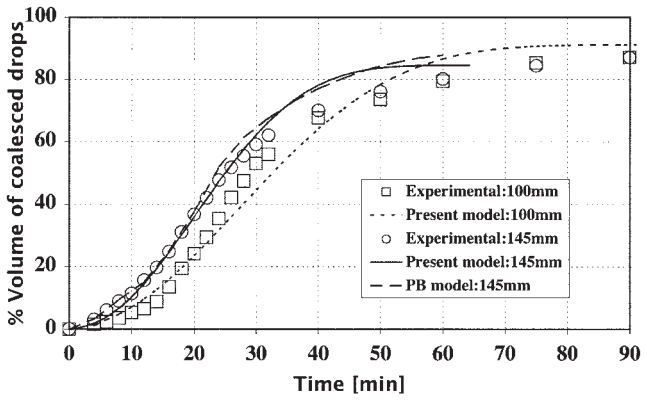


**Figure 11. Experimental (symbols) variation with time in % volume of propanediol drops coalesced during sedimentation in dispersions with different initial heights ($h_0$ = 100 and 145 mm, represented by squares and circles, respectively) and average drop diameter $d_0$ = 28 $\mu$m measured by Wang and Davis.[3]**

The simulation results of their population balance (PB) model and the present model are denoted by the dashed and full lines, respectively, for the dispersion with $h_0$ = 145 mm.

by Wang and Davis[3] by fitting the experimental data to the drop population balance model involving the numerical integration of the space- and time-dependent differential equations. The present simple model describes their experimental results as well as their population balance model. It should be mentioned that both models involve parameters that are determined by fitting the experimental data. However, their method involves adjusting the value of the Hamaker constant to allow for the van der Waals forces of attraction, and carrying out extensive computations of numerical differentiation of the large number of simultaneous differential equations by the finite-difference method until the calculated time-dependent variation in the volume of coalesced drops agrees with that measured experimentally. In contrast, the present analytical model is simple and does not involve extensive computations. Squares represent the experimental variation with time in the % volume of drops coalesced with their bulk homophase in a dispersion with identical initial conditions, except that the initial dispersion height is 100 mm. This is well described by the dotted line, which is the variation obtained by the present model using the values of the parameters $t_m$ and $t_f$ listed in Table 1. The calculated values of $d_m$, $v_0$, $\psi_0$, and $\tau_0$ are also listed. It is interesting to note that the maximum average drop diameter $d_m$ in the dispersion with a height of 145 mm is larger than that in the dispersion with a height of 100 mm. The corresponding time taken is shorter in the former case than that in the latter case. This is explained by the fact that the number of droplet collisions and, consequently, the droplet growth rate $(dd/dt)_0$ listed in Table 1 is larger in the taller dispersion than that in the shorter dispersion.

Their experimental results also indicate that the average drop diameter in the dispersion increases with time as a result of binary coalescence until a maximum value is reached; it decreases thereafter as large drops sediment out of dispersion, leaving behind smaller drops. This validates the assumption made in the model, which is applicable to present and published experimental data on dispersions involving a wide range of initial drop volume concentrations and size distributions.

It is clear from the present experimental results shown in Figure 4 and those of Wang and Davis[3] that the dispersions used are initially polydisperse, having a drop size distribution. The extent of polydispersity of the initial drop size distribution can be characterized by its standard deviation $\sigma$ and average diameter $d_0$ as done by Wang and Davis.[4] Their population balance simulation results showed that the larger the value of $\sigma/d_0$, the shorter is the time $t_m$ taken for the drops to grow to their maximum average diameter $d_m$, causing maximum phase separation rate during the temporal evolution. This is because a larger value of $\sigma/d_0$ corresponds to a larger spread in the initial drop size distribution, which results in larger relative creaming velocities of drops in many of the interacting size categories, leading to higher rates of gravitational interdrop collisions and coalescence.

The present model allowed for the effect of the temporal evolution of the average drop diameter (Eq. 2) on the rates of droplet creaming (Eq. 3b) and coalescence (Eq. 5a), resulting in Eqs. 8 and 9 for the time-dependent heights of the creaming and coalescing interfaces. The creaming velocity of drops of average diameter $d$ given by Eq. 3a (or 3b) was originally developed by Kumar and Hartland[12] based on experimental data for polydisperse dispersions. The temporal evolution of the average drop diameter given by Eq. 2 itself depends on the constants $c_1$, $c_2$, and $c_3$, which are affected by the polydispersity of the initial drop size distribution through the values of $t_m$ and $t_f$ for complete phase separation. The time $t_m$ taken for the drops to grow to their maximum average diameter, attributed to interdrop coalescence, corresponds to the inflection point on the variations in $h_s$ and $h_c$ with time given by Eqs. 8 and 9. Equation 10b, which is deduced from Eq. 8 and basically derived using Eqs. 2 and 3b, shows that the value of $t_m$ can be calculated if the value of $t_f$ is known. It also indicates that the shorter the time $t_m$ for the drops to grow to their maximum average diameter, the shorter is also the separation time $t_f$ for a given dispersion.

The initial polydispersity of the dispersion would affect the interdrop collisions and coalescence, which will be reflected in the measured values of $t_m$ and $t_f$. For instance, if the standard deviation $\sigma$ of the initial drop size distribution of a polydisperse dispersion with an average drop diameter $d_0$ is large, then the value of the measured time $t_m$ would be shorter according to the population balance simulation results of Wang and Davis[4] and so the value of the measured separation time $t_f$ would also be shorter, as predicted by Eq. 10b. The value of $t_f$ is obtained in the present work by fitting the experimental data of the variations with time in the heights $h_s$ and $h_c$ to Eqs. 8 and 9. As explained above, because these equations are obtained using Eq. 2 for temporal evolution of average drop diameter, and Eqs. 3b and 5a for creaming and coalescence rates involving the times $t_m$ and $t_f$, the effect of polydispersity is thus implicitly allowed. This is corroborated by the good agreement between the experimental results and those obtained using the present model shown in Figures 6, 7, and 11.

### *Comparison of experimental and predicted coalescence times*

The values of the initial interfacial coalescence times $\tau_0$ of drops of diameter $d_0$, calculated from Eq. 7b using the experimental data on dispersions, are listed in Table 1. The following analysis is presented to predict these coalescence times using a

theoretical equation on the drainage of the intervening continuous phase film between a drop and the bulk homophase.

Allowing for the surface mobility of drops, Davis et al.[8] analyzed the drainage of the continuous phase film of thickness $\delta$ at the apex during the approach of two spherical drops of diameters $d_1$ and $d_2$ with viscosity $\mu_d$ under the influence of the force $f$ and presented an analytical equation based on their numerical solution. Their analysis is further simplified[9] to give

$$-\frac{d\delta}{dt} = \frac{8f\sqrt{\delta}(\sqrt{\delta} + c)}{3\pi\mu_c d_e^2} \tag{15}$$

where $c = (0.6\mu_c/\mu_d)\sqrt{d_e}$, in which $d_e = 2d_1d_2/(d_1 + d_2)$ is the equivalent drop diameter.

When the force is constant, this integrates to give the coalescence time

$$\tau = \frac{3\pi\mu_c d_e^2}{4f} \ln\left(\frac{\sqrt{\delta_i} + c}{\sqrt{\delta_r} + c}\right) \tag{16a}$$

in which $\delta_i$ and $\delta_r$ are the initial and critical film thicknesses at rupture, respectively. The coalescence time $\tau_0$ of drops of diameter $d_0$ with the bulk homophase, at the coalescing interface in the droplet dispersions considered above, can be obtained by setting $d_1 = d_0$ and $d_2 = \infty$, so that $d_e = 2d_0$ to give

$$\tau_0 = \frac{3\pi\mu_c d_0^2}{f} \ln\left(\frac{\sqrt{\delta_i} + c}{\sqrt{\delta_r} + c}\right) \tag{16b}$$

in which $f = \pi\Delta\rho g d_0^3(1 - \varepsilon_0)/6(1 + 4.56\varepsilon_0^n)$ is the buoyancy force on the drops, where $n \approx 1$. This force is obtained from the analysis of Kumar and Hartland[12] for gravitational creaming or sedimenting drops involving extensive experimental data on dispersions. They argued that the buoyancy force on the lighter drops in a multidrop dispersion is lower than that on an isolated single lighter drop in the heavier continuous phase, given that the density of the dispersion is lower than that of the heavier continuous phase.

Drops of average diameter $d_0$ cream upward with a velocity $v_0$ because of the buoyancy force $f$. Because the total volume of a batch dispersion is constant, the upward creaming drops displace an equal volume of the continuous phase, which flows downward exerting a viscous drag force $f_d = 3\pi\mu_c d_0 v_0/(1 - \varepsilon_0)$ on the drops. If the drops do not coalesce upon impact with the coalescing interface of the homophase, their velocity and hence the drag force would both be reduced to zero at the coalescing interface. In any case, the continuous phase film between the drops and their bulk homophase drains under the influence of the buoyancy force $f$.

Table 1 lists the calculated values of the coalescence times $\tau_0$ of drops of diameter $d_0$ with their bulk homophase at the coalescing interface predicted by Eq. 16b, together with the values of the buoyancy force $f$. The initial film thickness $\delta_i$ is assumed to be equal to 400 nanometers, which is a typical measured value by Kumar et al.[13] during the drainage of thin aqueous films. The critical film thickness at rupture $\delta_r$ is set equal to 40 nanometers, which is the mean value obtained for aqueous films formed by a number of different coalescing oil drop systems.[14] As can be seen from Table 1, the values of the interfacial coalescence times $\tau_0$ predicted by Eq. 16b agree well with those obtained from the model Eq. 7b using the experimental data of the present work and those of Wang and Davis[3] on dispersions. The listed values of $Ca(\delta_i/2d_0)^2$ can be seen to be smaller than unity in most of the cases, indicating that the assumption of spherical drops in Eq. 16b is valid, in which $Ca = \mu_c v_0/\sigma$ is the capillary number. The interfacial coalescence time $\tau_0$ of single drops decreases by a factor of about 1.5 when the average drop diameter $d_0$ is approximately doubled.

## Summary and Conclusions

Only little experimental information is available on low Reynolds number droplet creaming or sedimentation in dispersions, which is important in many industrial applications. The theoretical analysis available is applicable only to dilute dispersions. This is mainly attributed to the lack of fundamental quantitative information on the effect of neighboring drops on the pairwise interdrop gravitational collision rates and efficiencies in concentrated dispersions. Therefore, this work considered concentrated rapeseed oil drops in water dispersions relevant to food processing. The effects of the size distribution and concentration of drops on the kinetics of low Reynolds number creaming, drop size growth resulting from interdrop coalescence, and interfacial coalescence are investigated. The drop size distributions are determined using a laser diffraction method, whereas the time-dependent concentrations of creaming drops along the height of dispersion are measured using a novel radioactive $\gamma$-ray attenuation technique. The time-dependent creaming velocity and coalescence rate increased initially, attributed to an increase in drop size by interdrop coalescence until their maximum values are attained, and decreased subsequently as larger drops creamed out of the dispersion, which is consistent with published data.[3] The times taken for the attainment of the maximum values, and completion of creaming and coalescence are shorter for concentrated dispersions in which the initial average diameter and concentration of drops are large.

A simple analytical model is presented, which describes well not only the present experimental data on concentrated dispersions but also those of Wang and Davis[3] on dilute dispersions. The results obtained by the simple model are in good agreement with those predicted by Wang and Davis[3] using the population balance model involving extensive numerical computations. The present simple model enabled the determination of interfacial coalescence times of single drops using experimental data on dispersions, which decreased with increasing average drop diameter. These are well predicted by the published[8,9] equation for drainage of the continuous phase film between the drop and its bulk homophase.

## Acknowledgments

The authors are thankful to Dr. Rok Gunde for the measurement of interfacial tensions. This paper is dedicated to the memory of Dr. Kurt May, who was involved in the design and development of the $\gamma$-ray density profile apparatus.

## Literature Cited

1. Jeelani SAK, Pandit A, Hartland S. Factors affecting the decay of batch liquid–liquid dispersions. *Canadian Journal of Chemical Engineering.* 1990;68:924-931.

2. Lobo L, Ivanov I, Wasan D. Dispersion coalescence: Kinetic stability of creamed dispersions. *AIChE Journal.* 1993;39:322-334.
3. Wang H, Davis RH. Experiments on phase separation of dilute dispersions of coalescing drops. *Journal of Colloid and Interface Science.* 1996;181:93-98.
4. Wang H, Davis RH. Simultaneous sedimentation and coalescence of a dilute dispersion of small drops. *Journal of Fluid Mechanics.* 1995; 295:247-261.
5. Reddy SR, Melik DH, Fogler HS. Emulsion stability—Theoretical studies on simultaneous flocculation and creaming. *Journal of Colloid and Interface Science.* 1981;82:116-127.
6. Zhang X, Davis RH. The rate of collisions due to Brownian or gravitational motion of small drops. *Journal of Fluid Mechanics.* 1991;230:479-504.
7. Panoussopoulos K. Separation of crude oil–water emulsions: Experimental techniques and models. PhD Dissertation, Zurich, Switzerland: Swiss Federal Institute of Technology; 1998.
8. Davis RH, Schonberg JA, Rallison JM. The lubrication force between two viscous drops. *Physics of Fluids.* 1989;A1:77-81.
9. Jeelani SAK, Hartland S. Effect of surface mobility on collision of spherical drops. *Journal of Colloid and Interface Science.* 1998;206: 83-93.
10. Hartland S, Vohra DK. Koaleszenz in vertikalen dichtgepackten Dispersionen. *Chemie Ingenieur Technik.* 1978;50:673-682.
11. Jeelani S, Hosig R, Windhab E. Phase separation stability of emulsions: Experiments and models. *Proceedings of 3rd World Congress on Emulsions*, Lyon, France, Sep. 24-27, 2002.
12. Kumar A, Hartland S. Gravity settling in liquid/liquid dispersions. *Canadian Journal of Chemical Engineering.* 1985;63:368–376.
13. Kumar K, Nikolov AD, Wasan DT. Effect of film curvature on drainage of thin liquid films. *Journal of Colloid and Interface Science.* 2002;256:194-200.
14. Jeelani SAK, Hartland S. Effect of interfacial mobility on thin film drainage. *Journal of Colloid and Interface Science.* 1994;164:296-308.

*Manuscript received Jun. 11, 2003, and revision received Apr. 28, 2004.*